EPJ Web of Conferences **29**, 00050 (2012)
DOI: 10.1051/epjconf/20122900050

Effect of sol-gel method on structural and electron magnetic resonance properties of $Pr_{0.6}Sr_{0.4}MnO_3$ manganite

R. Thaljaoui [1a,b,c], W. Boujelben[a], M. Pękała [b], J. Szydłowska[c] and A. Cheikhrouhou[a, d]

[a] Laboratoire de Physique des Matériaux, Faculté des Sciences de Sfax, B. P. 1171, 3000 Sfax Tunisia
[b] Faculty of Physics, Warsaw University of Technology, Koszykowa 75, 00-662 Warsaw, Poland.
[c] Department of Chemistry, University of Warsaw, Al. Zwirki i Wigury 101, 02-089, Warsaw, Poland.
[d] Institut NEEL, CNRS, B. P.166, 38042 Grenoble cedex 9, France

Abstract. Structural and electron magnetic resonance studies in a broad temperature range are reported for $Pr_{0.6}Sr_{0.4}MnO_3$ manganite synthesized by sol-gel method. Temperature dependence of magnetic resonance spectra is analyzed in the paramagnetic state and compared to similar systems. Using the temperature variation of signal intensity the activation energy is calculated.

1 Introduction

Perovskite manganites (ABO_3) with general formula $R_{1-x}A_xMnO_3$ (R=La,Pr etc. and A=Ca, Sr etc.,) have attracted much attention for interesting magnetic refrigeration based on the magnetocaloric effect [1]. Therefore, the materials with large magnetocaloric effect are actively searched and examined [2] on their higher energy efficiency and environmental friendliness superior to the conventional vapor-compression-based refrigeration. The discovery of the large magnetocaloric effect in the hole-doped perovskite manganites [3,4] as well as the observation of colossal magnetoresistance effect [5] in these materials, have attracted intensive interest [6-9]. The origin of the ferromagnetic state and metallicity has been explained on the basis of the double exchange (DE) and superexchange (SE) mechanisms. In many studies, it has been shown that the strength of DE and SE interactions in manganites is very sensitive to the variation of the average ionic radius of the A-site or Mn-site ions and the carrier density controlled by the Mn^{3+}/Mn^{4+} ratio [10] . In previous work we have reported the electron magnetic resonance of $Pr_{0.6}Sr_{0.4}MnO_3$ synthesized by conventional solid state method [11]. In order to understand the effect of the elaboration method on physical properties, the present work reports the properties of $Pr_{0.6}Sr_{0.4}MnO_3$ sample elaborated by sol gel method.

[1] e-mail : rachidthaljaoui@yahoo.fr

2 Experimental techniques

$Pr_{0.6}Sr_{0.4}MnO_3$ manganite with nanometer size crystallites was prepared by the sol-gel technique. Stoichiometric amounts of Pr_6O_{11}, $SrCO_3$ and Mn_2O_3, were dissolved in minimal amount of nitric acid to obtain a clear pink solution. Suitable amount of citric acid (CA) was employed as complexation agent (1.5 mol of citric acid corresponds to 1mol of metal cation). The resulting mixture was well magnetically stirred for 2 h in order to ensure complete dissolution of citric acid and to obtain stable metal–CA complexes. At this stage, the ethylene glycol (EG) was added to the solution as chelating agent. Then, the temperature was slowly increased to 90°C under constant stirring for about 4h to evaporate the excess solvent and to accelerate the poly-etherification reaction between CA and EG. When the solvent in the system was completely evaporated, a homogeneous red resin with a glassy appearance was obtained. This resin was then dried at 150°C for about 6h to evaporate the nitrogen and obtain a black fine powder which was then crushed and heated in air at 300°C before sintering at various temperatures (400°C-800°C) for 6h hours. After cooling, the sample was pressed into a pellet (of about 1mm thickness and 13mm diameter), and then sintered at 900 and 1000°C for 12h in air with intermediate regrinding and repelleting. Phase purity, homogeneity and cell dimensions were determined by powder X-ray diffraction at room temperature. Structural analysis was made using the standard Rielveld technique [12, 13]. Electron magnetic resonance measurements were performed with a Bruker spectrometer, operating at 9.44 GHz (X-band).

3 Structural studies

The room-temperature X-ray diffraction pattern of $Pr_{0.6}Sr_{0.4}MnO_3$ shown in Figure 1 indicates that our sample has a single phase and can be indexed in the orthorhombic structure with Pnma space group.

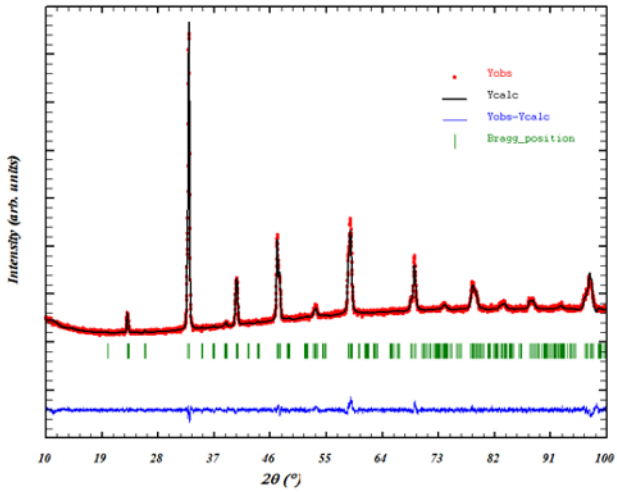

Fig. 1. Room - temperature X-ray diffraction pattern and refinement of $Pr_{0.6}Sr_{0.4}MnO_3$ manganite

The structural parameters were refined by the standard Rietveld technique. The quality of the refinement is evaluated through the indicator χ^2 equal to 1.59. Lattice parameters are found to be equal to a=5.4156(1) Å, b=7.6540(7) Å and c=5.4709(5) Å, the unit cell volume is equal to 227.436(4) $Å^3$. The unit cell parameters and volume are relatively reduced as compared to the values observed for polycrystalline $Pr_{0.6}Sr_{0.4}MnO_3$ manganite elaborated by the solid state reaction [11].

The average crystallite size was evaluated from a width of diffraction peaks using Sherrer formula [14] and is found to be equal to 26 nm.

4 EMR results

In Figure 2, we plot the electron magnetic resonance (EMR) spectra of the $Pr_{0.6}Sr_{0.4}MnO_3$ recorded in the temperature range 200 – 370 K. The maximum of intensity I(T) is observed at T= 250 K. This temperature is lower than 315 K found for the $Pr_{0.6}Sr_{0.4}MnO_3$ manganite elaborated by solid state method. In the paramagnetic phase the EMR spectrum consists of a single approximately symmetrical line with a shape close to a Lorentzian derivative. Using the EMR measurements the line width ΔH, the asymmetry, the intensity and the g_{eff} values were calculated. ΔH is deduced from the peak-to-peak distance between the maximum and the minimum of the derivative of the EMR absorption, the asymmetry is defined by the maximum to minimum ratio. The intensity of the response is defined by $\beta(\Delta H)^2$, where β is the peak amplitude. The g_{eff} value is determined via the following equation:

$$g_{eff} = h\upsilon/\mu_B H_{res} \quad (1)$$

where h is the Planck constant, μ_B is the Bohr magneton, υ is the frequency and H_{res} is the resonance field.

We should note that the resonance field diminishes slowly in the paramagnetic phase from 3366 Oe at 370 K down to 3348 Oe at 200 K. The similar behavior was reported by R. Thaljaoui et al. [11] for $Pr_{0.6}Sr_{0.4}MnO_3$ manganite prepared by solid state reaction with mean crystallite size of 41 nm.

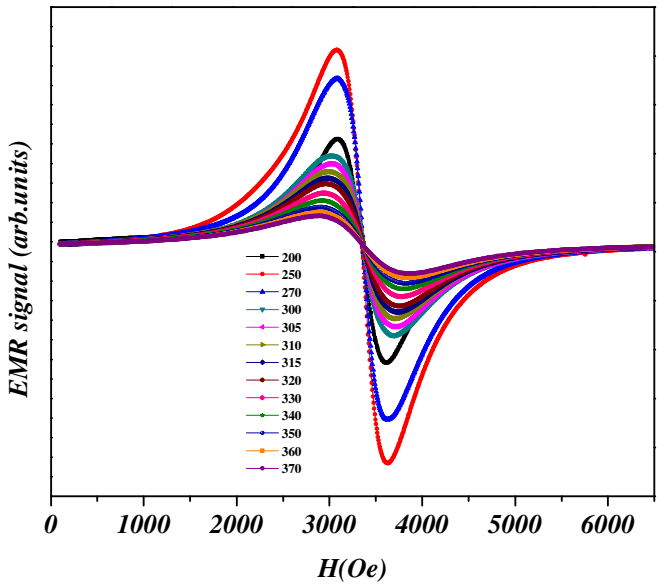

Fig. 2. Electron magnetic resonance spectra of $Pr_{0.6}Sr_{0.4}MnO_3$ manganite

We plot in Figure 3 the temperature dependence of g_{eff}. One may see that at T=370 K the corresponding value of g_{eff} is equal to 2.00054, which falls into a range characteristic for doped manganites in the paramagnetic state [15, 16]. We should also note that the line width ΔH is a non monotonic function of temperature (not plotted) for a broad temperature interval. The ΔH exhibits a minimum at 310K. One may conclude that a transition temperature is located somewhat below 310K as it is observed in manganites [11, 17].

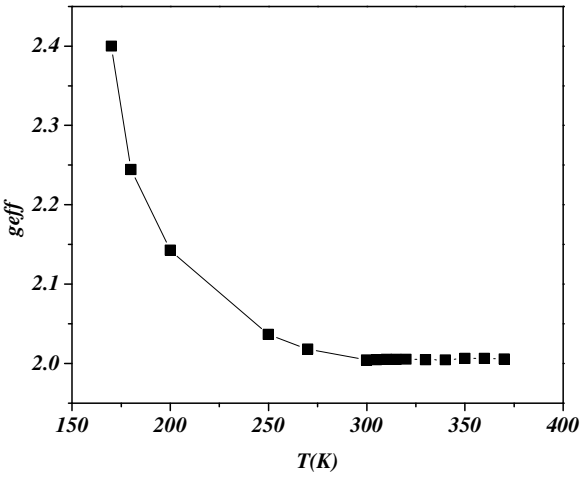

Fig. 3. Temperature dependence of g_{eff} of $Pr_{0.6}Sr_{0.4}MnO_3$ manganite

Figure 4 shows the temperature variation of signal intensity I(T). In the ferromagnetic phase the signal intensity is an abruptly diminishing function of temperature. In the paramagnetic phase I(T) increases slowly. A similar behavior was observed for $Pr_{0.6}Sr_{0.4}MnO_3$ manganite prepared by solid state reaction [11].

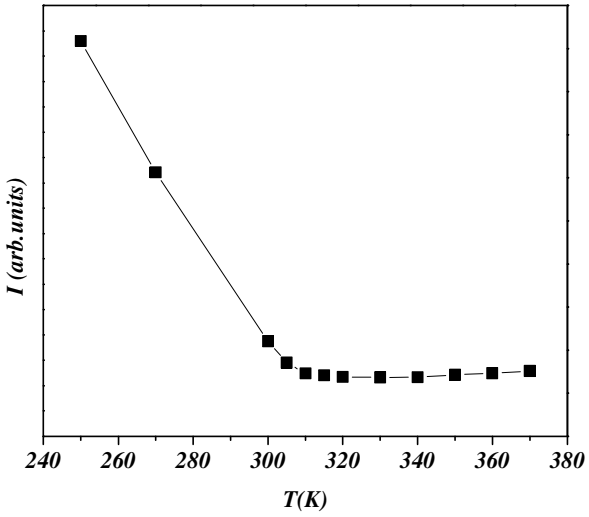

Fig. 4. Temperature dependence of signal intensity of $Pr_{0.6}Sr_{0.4}MnO_3$ manganite

Above 250 K the intensity diminishes abruptly with temperature rising up to 310 K, reaches a minimum and then increases slowly. One should notice that the accuracy of applied I (T) calculation is high enough only in paramagnetic phase, where signals are more symmetric (Figure 5). Therefore the I(T) dependence below T_C offers only a rough approximation. In the paramagnetic phase the evolution of the signal intensity versus temperature can be expressed as follows:

$$I(T) = I_0 \exp(E_1/k_BT) \quad (2)$$

where k_B is the Boltzmann constant and E_1 is the activation energy. The activation energy E_1 equal to 67.6 meV was deduced from Ln(I) versus 1/T dependence. Such activation energy is somewhat smaller than values reported for similar manganites [11].

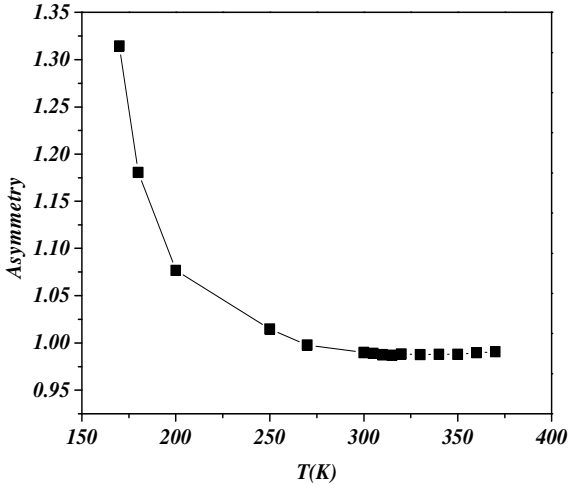

Fig. 5. Temperature dependence of signal asymmetry of $Pr_{0.6}Sr_{0.4}MnO_3$ manganite

5 Conclusions

The structural study shows that our present sample crystallizes in the orthorhombic structure with *Pnma* space group and the mean crystallite size is about 26 nm. Rietveld refinement indicates a decrease in the lattice volume of our sample compared to the manganite $Pr_{0.6}Sr_{0.4}MnO_3$ prepared by solid state reaction.

The transition temperature is somewhat lower as compared to the $Pr_{0.6}Sr_{0.4}MnO_3$ manganite prepared by the solid state method. It can be related to the influence of sol-gel method on grain size and its distribution. In the paramagnetic phase the EMR spectra consists of a single line with a shape close to a Lorentzian one and the resonance field corresponds to a geff factor close to 2 and is temperature independent.

Acknowledgements

This work was supported by the Tunisian Ministry of Higher Education and Scientific Research and the Ministry of Science and Higher Education of Poland.

References

1. A. M. Tishin, Y. I. Spichkin, The Magnetocaloric Effect and Its Applications, Institute of Physics, Bristol, 2003.
2. E. P. Nobrega, N. A. de Oliveira, P. J Von Ranke and A. Troper, J. Phys.: Condens. Matter **18** (2006) 1275–128.
3. X. X. Zhang, J. Taiada, Y. Xin, G. F. Sunm, K. W. Wong, X. Bohigas, Appl. Phys. Lett. **69** (1996) 3596.
4. Z. B. Guo, Y. W. Du, J. S. Zhu, H. Huang, W. P. Ding, D. Feng, Phys. Rev. Lett. **78** (1997) 1142.

5. C. N. R. Rao, B. Raveau (Eds.), Colossal Magnetoresistance, Charge Ordering and Related Properties of Manganese Oxides, World Scientific, Singapore, 1998.
6. P. K. Siwach, H. K. Singh, O. N Srivastava, J. Phys.: Condens. Matter **20** (2008) 273201.
7. R. N. Mahato, K. Sethupathi, V. Sankaranarayanan, R. Nirmala, J. Magn. Magn. Mater. **322** (2010) 2537.
8. D. H. Manh, P.T. Phong, T. D. Thanh, L.V. Hong, N. X. Phuc, J. Alloys Compd. **499** (2010) 131.
9. V. P. S. Awana, R. Tripathi, N. Kumar, H. Kishan, G.L. Bhalla, R. Zeng, L.S. Sharth Chandra, V. Ganesan, H.U. Habermeier, J. Appl. Phys. **107** (2010) 09D723.
10. P. G. Radaelli, M. Marezio, H.Y. Hwang, S.W. Cheong, J. Solid State Chem. **122** (1996) 444.
11. R. Thaljaoui, W. Boujelben, M. Pękała, J. Szydłowska, A. Cheikhrouhou, J. Alloys Compd. **526** (2012) 98.
12. H. M. Rietveld, J. App. Cryst. **2** (1969) 65.
13. T. Roisnel, J. Rodriguez-Carvajal, Computer program FULLPROF, LLB-LCSIM. May 2003.
14. A. Taylor, X-ray Metallography, Wiley, New York, 1961
15. C. Autret, M. Gervais, F. Gervais, N. Raimboux, P. Simon, Solid State Sciences **6** (2004) 815
16. J. Gutiérrez, V. Siruguri, J.M. Barandiarán, A. Peña, L. Lezama, T. Rojo, Physica B **372** (2006) 173.
17. T.L. Phan, N.D. Tho, L.V. Bau, N.X. Phuc, S.C. Yu, J. Magn. Magn. Mater. **303** (2006) e339–e341